Insect Biochemistry and Molecular Biology 39 (2009) 440–447

Contents lists available at ScienceDirect

Insect Biochemistry and Molecular Biology

journal homepage: www.elsevier.com/locate/ibmb

Binding specificity of locust odorant binding protein and its key binding site for initial recognition of alcohols

Quan-Yong Jiang [a,1], Wei-Xuan Wang [b,1], Ziding Zhang [b,**], Long Zhang [a,*]

[a] Key Lab for Biological Control of the Ministry of Agriculture, China Agricultural University, Beijing 100193, China
[b] State Key Laboratory for AgroBiotechnology, College of Biological Sciences, China Agricultural University, Beijing 100193, China

ARTICLE INFO

Article history:
Received 12 January 2009
Accepted 7 April 2009

Keywords:
Odorant binding protein
Binding specificity
Locusta migratoria
Homology modeling
Molecular docking
Site-directed mutagenesis
Binding sites

ABSTRACT

Odorant binding proteins (OBPs) are required for olfaction perception, and thus may be possible targets for controlling the population of pests by interfering with their chemical communication. A single OBP LmigOBP1 has been identified in the antennae of *Locusta migratoria*, though four isoforms have been detected. Here, we have investigated the ligand-binding specificity of LmigOBP1 using 67 volatile odor compounds. Fluorescence assays indicate that LmigOBP1 does not bind fecal volatiles or green leaf odors, but shows high affinity for some linear aliphatic compounds, with pentadecanol and 2-pentadecanone being the strongest binding ligands. A 3-dimensional (3D) model of LmigOBP1 was built by homology modeling. Docking simulations based on this model suggested that Asn74 of LmigOBP1 is a key binding site, and this was validated by site-directed mutagenesis and fluorescence assays. We suggest that, as a general rule, a hydrophilic amino acid at the entrance of the binding cavity participates in initial recognition of ligands, and contributes to ligand-binding specificity of OBPs.

1. Introduction

Olfactory stimuli play a major role in insect behaviors such as host-seeking, enemy-defending, mating, aggregation and migration. For example, *Locusta migratoria*, a notorious worldwide agricultural pest, uses olfactory cues to aggregate and shift from a solitary to a gregarious phase. Therefore, a better understanding of the olfactory system of the locust and other insects could help in devising strategies to disrupt their aggregation behavior.

Recognition and discrimination of odorants is a complex process involving the peripheral excitation of olfactory neurons, followed by signal processing in antennal lobes, mushroom bodies and central nervous areas. Odorant binding proteins (OBPs) fill the sensillar space and interact with odorants and pheromones (Vogt and Riddiford, 1981; Vogt et al., 1991; Krieger and Breer, 1999; Pelosi et al., 2006). Although the precise physiological role of these proteins is not completely understood, they are strongly suggested to be involved in the binding and transport of odors through the sensillum lymph to specific odorant receptors (ORs) localized in the membrane of olfactory neurons (Prestwich et al., 1995). Recently OBPs have been shown to be required for correct functioning of the olfactory system in insects (Xu et al., 2005; Matsuo et al., 2007), and therefore could represent interesting targets for interfering with odor perception in species of economical interest (Bau et al., 1999; Riba et al., 2001; Quero et al., 2004).

Since the discovery of OBPs, their ability to bind small organic compounds has been used as a tool to understand their physiological functions. The first insect OBP was identified in the moth *Antheraea polyphemus* by its affinity for a tritium-labeled pheromone (Vogt and Riddiford, 1981). This method was also used to evaluate ligand-binding specificities of OBPs. Binding assays using two tritium-labeled pheromones revealed that two pheromone-binding proteins (PBPs) from *Antheraea pernyi* (AperPBP1 and AperPBP2) showed a >1000-fold range of binding affinities among ligands with very similar structures (Du and Prestwich, 1995). Competitive binding data of *A. polyphemus* PBPs (ApolPBP1, 2 and 3) with tritium-labeled pheromone components indicated binding preferences for a specific pheromone component for each of the three PBP-subtypes (1–3). This supports the idea that PBPs contribute to odor discrimination (Maida et al., 2000, 2003). Fluorescence binding assays were used to study the binding of OBPs to putative ligands. *Mamestra brassicae* MbraPBP1 bound all three components of the pheromones *cis*-11-hexadecenol, *cis*-11-hexadecenal and *cis*-11-hexadecenyl acetate, with dissociation constants of 0.17, 0.29 and 0.20 μM, respectively (Campannacci et al., 2001; Bette et al., 2002). ApolPBP1 binds a specific pheromone and a series of structurally related compounds with similar

* Corresponding author. Fax: +86 10 62731048.
** Corresponding author. Fax: +86 10 62731332.
E-mail addresses: zidingzhang@cau.edu.cn (Z. Zhang), locust@cau.edu.cn (L. Zhang).
[1] Q.-Y. Jiang and W.-X. Wang contributed equally to this work.

0965-1748/$ – see front matter © 2009 Elsevier Ltd. All rights reserved.
doi:10.1016/j.ibmb.2009.04.004

affinities (Campannacci et al., 2001). These results indicate a rather broad ligand-binding specificity, in contrast with the high selectivity exhibited by insects in recognizing their specific pheromones.

Three-dimensional structures of complexes of OBPs and ligands provide evidence for ligand-binding specificity. The crystal structure of *Bombyx mori* pheromone-binding protein (BmorPBP) bound to bombykol revealed that bombykol interacts with the binding cavity through numerous hydrophobic interactions (Sandler et al., 2000). Analysis of the crystal structures of *Drosophila melanogaster* OBP LUSH bound with small alcohols, such as ethanol, propanol and butanol, showed that the residues Thr48, Ser52 and Thr57 are involved in the interactions with alcohol ligands (Kruse et al., 2003). The amino acid residue Thr57 has been identified as the most critical residue for binding alcohols (Thode et al., 2008).

In *L. migratoria*, only one OBP has been identified along with four isoforms (Ban et al., 2003; Yu et al., 2007). Immunocytochemistry experiments have revealed that LmigOBP1 is expressed in the sensillum lymph of sensilla trichodea and basiconica (Jin et al., 2005). In Lepidoptera, sensilla trichodea are sensitive to pheromones, and express pheromone-sensitive PBPs, while most sensilla basiconica, which respond to general odorants but not known pheromones, mainly express general odorant binding proteins (GOBPs) (Steinbrecht et al., 1995; Zhang et al., 2001). Therefore, LmigOBP1 may play an important role in locust pheromone chemosensing. Although a few competitive binding assays with ligands have been reported for LmigOBP1 (Ban et al., 2003), its binding specificity and physiological function are not clear.

Here, we characterize the ligand-binding specificity of LmigOBP1 using 67 diverse small organic compounds. Based on the results, we combined docking simulations, site-directed mutagenesis and binding experiments to describe its binding sites, and propose a ligand-binding mechanism.

2. Materials and methods

2.1. Materials

A battery of 67 compounds was used to investigate ligand-binding specificity of LmigOBP1 (see Table 1). Ligands were purchased from Sigma–Aldrich, Fluka, Acros and TCI Corporations with the highest purity and stored as specified by the manufacturer.

2.2. Synthesis and purification of LmigOBP1

LmigOBP1 was obtained by bacterial expression, as previously described (Ban et al., 2003). This method produced the polypeptide in high yield (10 mg/l). An initial methionine residue was the sole modification with respect to the native protein. The recombinant OBP, which was present exclusive in inclusion bodies, was solubilized by treatment with urea and DTT, renatured by extensive dialysis, and purified by two chromatographic steps on the anion-exchange resin DE-52, followed by gel filtration on Superose-12, as previously described (Ban et al., 2003). The protein was >95% pure by SDS-polyacrylamide gel electrophoresis (SDS-PAGE), and the correct pairing of the three disulfide bridges was verified by mass spectrometry. The concentration of the purified recombinant LmigOBP1 was calculated from the absorbance at 280 nm, using the theoretical molar extinction coefficient of 7450 M^{-1} cm^{-1}. The value was calculated with the Protparam program on the ExPASy molecular biology server of the Swiss Institute of Bioinformatics, according to the algorithm of Gill and Hippel (1989).

2.3. Fluorescence assays

Fluorescence measurements were performed as reported previously (Ban et al., 2003), on a PerkinElmer LS 55 spectrofluorimeter in a 1 cm light-path fluorimeter quartz cuvette at 25 °C. N-phenyl-1-naphthylamine (1-NPN) was dissolved in methanol to yield a 1 mM stock solution. Fluorescence of 1-NPN was excited at 337 nm and emission was recorded between 370 and 470 nm. Spectra were recorded with a scan speed of 300 nm/min and three accumulations. The slit width used for excitation and emission was 10 nm. All ligands used in competition experiments were dissolved in HPLC purity grade methanol. Binding data were collected as three independent measurements.

Concentrations of competitors that caused a reduction of fluorescence to half-maximal intensity (IC_{50} values) were taken as a measure of binding dissociation constants were calculated from the corresponding IC_{50} values using the formula: $K_i = [IC_{50}]/(1 + [1\text{-NPN}]/K_{1\text{-NPN}})$, [1-NPN] being the free concentration of 1-NPN and $K_{1\text{-NPN}}$ being the dissociation constant of the complex LmigOBP1/1-NPN, which was calculated from the binding curve using the computer program Prism 5.0 Trial (GraphPad Software Inc.).

2.4. Three-dimensional structure modeling and molecular docking

A blast search (Altschul et al., 1990) of the amino acid sequence of LmigOBP1 was conducted against the current Protein Data Bank (PDB; http://www.rcsb.org) to find structural templates. In addition, based on the results of the fluorescence binding assays, we used the crystal structure of the bee *Apis mellifera* antennal pheromone-binding protein (AmelPBP) complexed with hexadecanoic acid (3BFH) as the template to build the 3D structure of LmigOBP1. Several initial models were constructed, using Modeler module (Sali and Blundell, 1993) in Discovery Studio 2.0 (Accelrys Software Inc.), and the one with the highest score of Profiles-3D (Luthy et al., 1992) was retained. To refine the initial homology model, the CHARMm (Brooks et al., 1983) force field was employed and the following three energy minimization procedures were processed. First, minimization was carried out while all of the hydrogen atoms were relaxed and the other atoms were fixed. Then, the side-chains were energy-minimized while the main chain was restrained. Finally, minimization was performed while all the atoms were relaxed. In each minimization procedure, two methods were used: the steepest descent method for 500 steps, followed by the conjugated gradient minimization for another 500 steps. The non-bond cutoff distance of 14 Å was used, and the long-range electrostatic interaction was calculated using the spherical cutoff method. The SHAKE algorithm (Rychaert et al., 1977) was applied to constrain the covalent bonds to hydrogen atoms during the minimization. Finally, the Profiles-3D method was used to evaluate the fitness between the sequence and the current 3D model.

Using the established homology model, a CHARMm-based docking program CDOCK (Wu et al., 2003) was employed to find the potential binding mode between LmigOBP1 and the ligand pentadecanol. The 3D structure of pentadecanol was sketched and further refined with a steepest descent minimization for 2000 steps, followed by a gradient minimization for another 2000 steps, using the CHARMm force field. The active site pocket of the receptor was found automatically by the Discovery Studio 2.0, and the location of the ligand hexadecanoic acid in 3BFH was also referenced for additional information. A site sphere radius of 10 Å was set to assign the entire pentadecanol binding pocket. Other parameters were set as default. The top 20 docking poses ranked by

Table 1
Binding affinities of ligands to LmigOBP1. Values are means of three independent experiments.

Ligands	Source	K_i (μM)	Ligands	Source	K_i (μM)
Aliphatic alcohols			*Aliphatic ester derivatives*		
cis-3-hexenol (C6)	P	–	Ethyl *cis*-3-hexenoate (C8)		–
2-Hexanol (C6)		–	Ethyl caprylate (C10)		1.17 ± 0.27
3-Hexanol (C6)		–	Ethyl nonanoate (C11)		2.45 ± 0.79
3-Octanol (C8)		–	Ethyl caprate (C12)		3.87 ± 0.55
Nonanol (C9)		–	Ethyl undecanoate (C13)		1.57 ± 0.28
5-Nonanol (C9)		–	Ethyl dodecanoate (C14)		1.11 ± 0.30
Linalool (C10)	P	–	Ethyl tridecanoate (C15)		1.16 ± 0.24
3,7-Dimethyl octanol (C10)		–	Ethyl myristate (C16)		1.70 ± 0.41
cis-3,7-Dimethyl-2,6-octadien-1-ol (C10)		–	Ethyl palmitate (C18)		–
10-Undecylenylalcohol (C11)		10.75 ± 0.74	Oleamide (C18)		5.55 ± 1.38
Undecanol (C11)		9.41 ± 2.79	Ethyl sterate (C20)		–
2,2,4-Trimethyl-3-nonanol (C12)		–	*Aliphatic acids*		
Dodecanol (C12)		7.20 ± 1.26	Pentadecanoic acid (C15)		7.33 ± 1.08
Tridecanol (C13)		3.48 ± 1.35	*Orbicular compounds*		
Tetradecanol (C14)		1.30 ± 0.18	Cyclohexanol (C6)	F	–
Pentadecanol (C15)		0.59 ± 0.19	3,5-Dimethyl cyclohexanol (C8)		–
Hexadecanol (C16)		1.70 ± 0.37	2,6-Dimethyl cyclohexanone (C8)		–
Heptadecanol (C17)		1.45 ± 0.65	2,6,6-Trimethyl-2-cyclohexene-1,4-dione (C9)	F	–
Aliphatic ketones					
2-Heptaone (C7)	F	–	*Heterocyclic compounds*		
2,6-Dimethyl-4-heptanone (C9)		–	2,5-Dimetylpyrazine (C6)	F	–
2-Undecanone (C11)		–	1-Aminoanthracen (C14)		–
6-Undecanone (C11)		–	*Aromatic compounds*		
2-Dodecanone (C12)		4.45 ± 0.48	Benzaldehyde (C7)	F,P	–
2-Tridocanone (C13)		2.08 ± 0.50	Benzyl alcohol (C7)	F,P	–
2-Pentadecanone (C15)		0.58 ± 0.19	Guaicacol (C7)	F	–
2-Hexadecanone (C16)		0.68 ± 0.06	DL-sec-phenethyl alcohol (C8)	F	–
2-Heptadecanone (C17)		0.62 ± 0.06	Acetophenone (C8)	P	–
Aliphatic aldehydes			4-Allyl-2-methoxyphenol (C10)		–
Hexanal (C6)	F,P	–	Benzenebutanol (C10)		–
trans-2-Hexenal (C6)	F,P	–	4-Tert-butylphenol (C10)		–
Octanal (C8)	P	–	α-Cymophenol (C10)		–
Nonanal (C9)	F,P	–	Dimethyl phthalate (C10)		–
Decanal (C10)	P	–	Diethyl phthalate (C12)		–
Undecylic aldehyde (C11)		–	α-Amylcinnamaldehyde (C14)		–
Dodecanal (C12)		–	Dibutyl phthalate (C16)		3.40 ± 0.91
Tridecanal (C13)		1.38 ± 0.59	Di (.alpha.-ethylhexyl) phthalate (C24)		–

Dissociation constants of ligands whose IC_{50} exceed 20 μM are represented as"–". Compounds from locust fecal volatils are represented as "F", and compounds from leaf of green plants, maize, corn, wheat are represented as "P".

the corresponding values of CHARMm energy were preserved to find the most probable binding mode.

2.5. Site-directed mutagenesis and expression of mutants

The LmigOBP1 coding sequence was mutated to yield the three mutants LmigOBP1 S59A (serine to alanine at position 59), LmigOBP1 N74A (asparagine to alanine at position 74), and LmigOBP1 V87A (valine to alanine at position 87). Mutations were generated using the quick-change mutagenesis PCR kit (Stratagene) with *Pfu* turbo DNA polymerase, the pET 5b/LmigOBP1 cDNA as template. The primers were synthesized according to Stratagene's web-based QuikChange® Primer Design Program at http://www.stratagene.com/qcprimerdesign. The correct insertion of mutations was verified by DNA sequencing. *Escherichia coli* (DE3) competent cells were transformed with the plasmids pET 5b/LmigOBP1 S59A, pET 5b/LmigOBP1 N74A and pET 5b/LmigOBP1 V87A. Expression of the proteins was induced by addition of IPTG, following the published protocol (Ban et al., 2003).

SDS-PAGE was used to monitor protein expression and purification. Mutations that were >95% pure by SDS-PAGE were identified, and their secondary structures were determined by circular dichroism (CD). The CD spectra were measured on a JASCO J-81 spectropolarimeter with 0.3 mg/ml of proteins in 50 mM Na phosphate, pH 7.4, at 25 °C between 180 and 260 nm, respectively. Purified mutations with correct secondary structures were used in fluorescence binding assays, as described above.

3. Results

3.1. Binding specificity of LmigOBP1

When excited at 337 nm, 1-NPN displayed an emission peak at 460 nm, which shifted to about 400 nm in the presence of LmigOBP1, with a 5-fold increase in intensity. Using these conditions, we measured a dissociation constant of the LmigOBP1/1-NPN complex of 3.83 ± 0.23 μM.

Under the hypothesis that LmigOBP1 may be important for locusts to detect semiochemicals, we tested 12 locust fecal components (Yu et al., 2007) and 10 leaf volatiles from barley, wheat (Shibamoto et al., 2007) and corn (Konstantopoulou et al., 2004). The natural sources of tested compounds are listed in Table 1. These ligands failed to compete for the binding of 1-NPN to LmigOBP1. Compounds having cyclic or heterocyclic structure also proved to be inefficient in binding (Table 1).

In contrast, aliphatic alcohols, ketones and esters exhibited good affinity for LmigOBP1 (Fig. 1). C6-C17 aliphatic alcohols showed different binding activities. The small compounds (C6–C10), failed to displace 1-NPN from LmigOBP1. Larger compounds (C11–C17) showed competitive ability. Binding affinities of C11–C15 aliphatic alcohols ranged from 10.75 ± 0.74 μM to 0.59 ± 0.19 μM. The highest binding affinity for LmigOBP1 was found using a C15 aliphatic alcohol pentadecanol. Aliphatic alcohols having longer carbon chain lengths (C16 or C17) showed weaker binding affinity, suggesting that C-15 aliphatic alcohols are good candidate ligands for LmigOBP1.

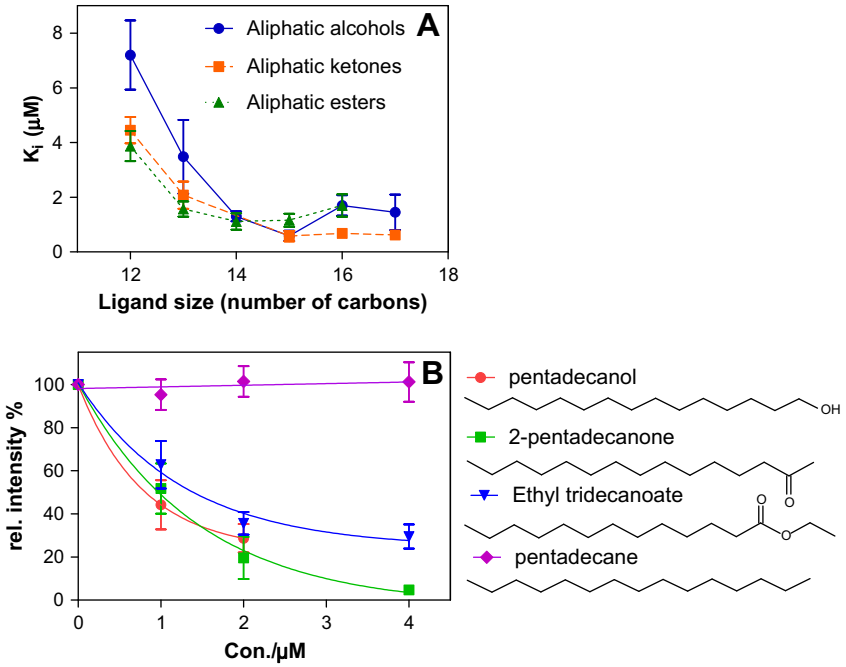

Fig. 1. Binding selectivity of LmigOBP1 by functional group and ligand size. (A) Relationship between ligand size and K_i of aliphatic alcohols (●), aliphatic ketones (■) and aliphatic ethyl esters (▲). Dissociation constants are the result of 1-NPN competition experiments (Table 1) with LmigOBP1. (B) Relationship between functional groups of ligands and competitive abilities. Pentadecanol (●), 2-pentadecanone (■), ethyl tridecanoate (▼), pentadecane (◆). Each ligand was incubated with 2 μM OBP and 2 μM 1-NPN at increasing concentrations. Fluorescence intensity values were normalized and plotted against total ligand concentrations. All spectra were subjected to background subtraction. Data are an average of three independent measurements and error bars represent the standard deviations of the mean derived from the differences between the measurements.

C7–C11 aliphatic ketones did not displace 1-NPN. Aliphatic ketones having longer carbon chain lengths (C12–C17) showed high binding affinities, in the range of 4.45 ± 0.48 μM–0.58 ± 0.19 μM. Similarly, small size aliphatic aldehydes had no competitive ability against 1-NPN. The compound tridecanal (C-13) also showed moderate binding. C10–C16 aliphatic esters bound to LmigOBP1 with binding affinities between 3.87 ± 0.55 μM and 1.11 ± 0.30 μM. Aliphatic esters with less than C-10, or more than C-16 chain lengths did not show competitive binding ability, with the exception of oleamide with a binding affinity of 5.55 ± 1.38 μM.

Taken together, the binding data showed that among a large number of possible ligands, LmigOBP1 interacted preferentially with aliphatic alcohols and ketones of around C15 length, with binding affinities to pentadecanol and 2-pentadecanone being particularly high. These results suggested that linear aliphatic compounds of 15 carbon chains are suitable for binding to LmigOBP1. Another two C15 aliphatic compounds, aliphatic alkyl (pentadecane) and aliphatic acid (pentadecanoic acid), were tested. Pentadecane failed to compete with 1-NPN for LmigOBP1, even when its concentration reached 100 μM. Pentadecanoic acid was a weak competitor with a binding affinity of only 7.33 ± 1.08 μM. These results suggested that the polar terminal C–O group is a key factor for effective binding to LmigOBP1.

3.2. 3D model of LmigOBP1

By blast searching, six structurally determined OBPs, including *B. mori* PBP (BmorPBP), *Drosophila* OBP (LUSH), cockroach *Leucophaea maderae* PBP, honeybee *A. mellifera* OBP (AmelPBP), giant silk moth *A. polyphemus* OBP (ApolPBP1) and *Anopheles Gambiae* OBP (AgamOBP) were found to share sequence similarity with LmigOBP1. Classified into the insect pheromone/odorant-binding protein superfamily, these six OBPs share a similar structural fold and can be used as the structural template in the homology modeling of LmigOBP1. Although AgamOBP had the highest sequence similarity with LmigOBP1 (27% sequence identity and an *E*-value of 3.0E-13), the complex of AmelPBP-hexadecanoic acid (pdb code 3BFH, 24% sequence identity and *E*-value of 1.0E-5) was chosen as the template because the available ligand structure in 3BFH had a structure similar to pentadecanol. Using the selected structural template and the established sequence alignment, the predicted 3D model of LmigOBP1 was generated by Modeler. As shown in Fig. 2A, the last 10 amino acids in the LmigOBP1 C-terminus were not matched. At the time of analysis, no available OBP X-ray crystal structures had such long C-termini, so the structure of these C-terminal residues was left out of the established 3D model. After structural refinement, the Verify Score of the final LmigOBP1 model by Profiles-3D was 43.28, implying that the overall quality of the predicted LmigOBP1 structure was generally reliable. In addition, the heavy atoms root mean square deviation (RMSD) between the model and the template was 1.25 Å, indicating that the changes between the model and the template in the overall structure were negligible (Fig. 2B).

The predicted 3D structure of LmigOBP1 consisted of six α-helices located between residues 10–24 (α1), 29–37 (α2), 44–55 (α3), 68–74 (α4), 80–90 (α5), and 98–112 (α6). Three pairs of disulfide bridges connected Cys21 in α1 and Cys52 in α3, Cys48 in α3 and Cys99 in α6, Cys90 in α5 and Cys108 in α6 (Fig. 2C). In addition, the 3D structural model of LmigOBP1 showed a large pocket formed by all α helices except α2 (Fig. 2D). In this model, most of the residues forming the pocket were found to be hydrophobic (valine, leucine, isoleucine, methionine and phenylalanine). However, some hydrophilic residues (asparagine, tyrosine and serine) were also present in the binding site, and probably responsible for hydrogen bonding with the functional group of the ligand.

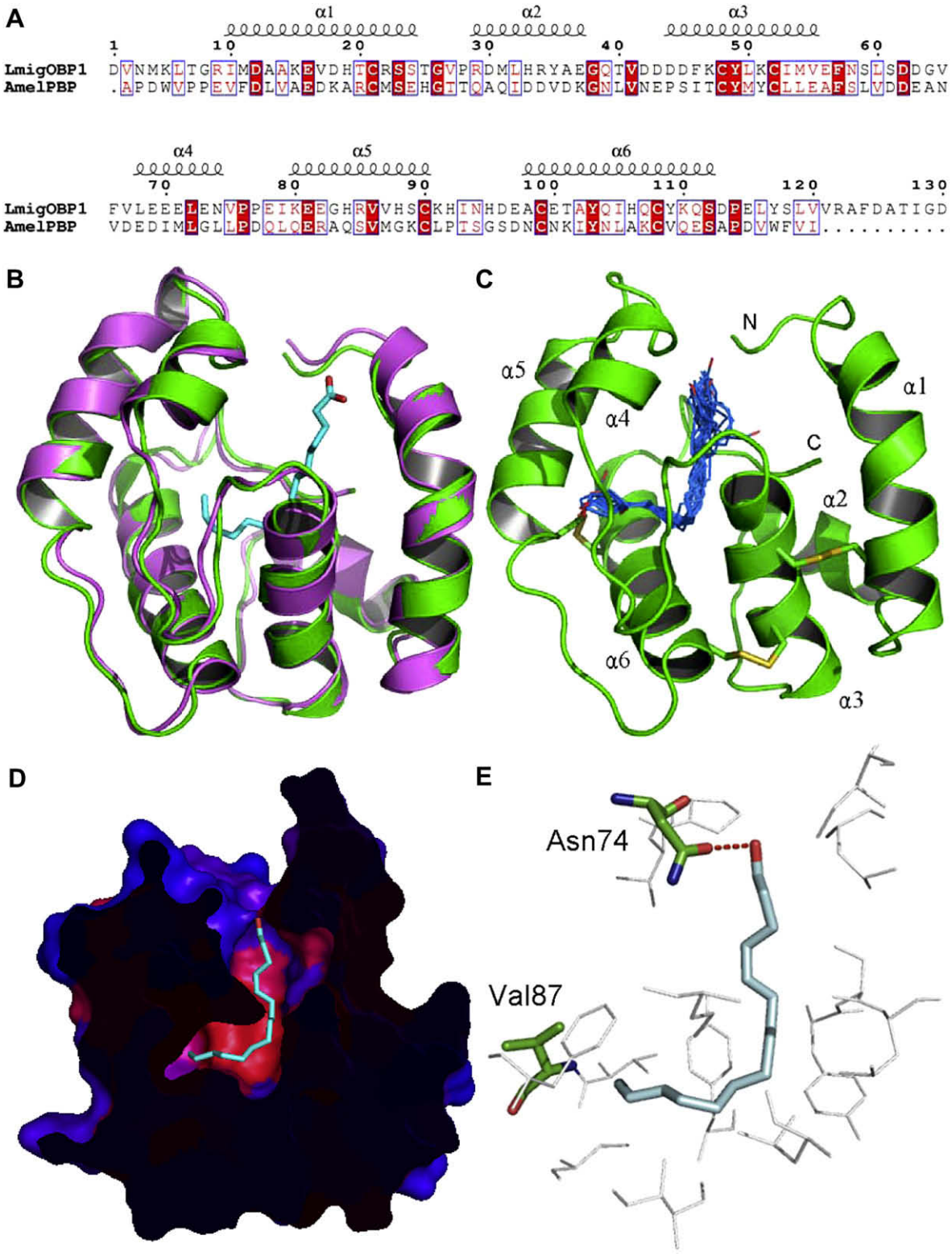

Fig. 2. Three-dimensional structure and docking experiments of LmigOBP1. (A) Sequence alignment of LmigOBP1 and AmelPBP. The secondary structure elements for AgamOBP1 are shown above the sequences. α-helices are displayed as squiggles. Strictly identical residues are highlighted in white letters with a red background. Residues with similar physico-chemical properties are shown in red letters. Alignment positions are framed in blue if the corresponding residues are identical or similar. (B) Superimposed structures of AmelPBP and LmigOBP1. The model of LmigOBP1 and crystal structures of AmelPBP are shown in green and magenta, respectively. Hexadecanoic acid is shown as a stick. (C) Overall structure of the LmigOBP1 and the docking result. Disulfide bridges are shown as sticks, helices and the two termini are labeled. The top 20 docking poses are shown as stick models. Images were generated using Pymol (www.pymol.org). (D) The binding pocket of LmigOBP1 and the docking result, with pentadecanol shown as a stick model with the hydroxyl oxygen in red. The color of the pocket surface is according to hydrophobicity, with high hydrophobicity in red and low in blue. (E) A close view of the potential binding mode of LmigOBP1 with pentadecanol. Pentadecanol and the residues that were determined to be important for ligand binding are represented as stick models. Residues shown as line drawings have a distance to pentadecanol of less than 4 Å. Hydrogen bonds are shown as dashed lines. (For interpretation of the references to colour in this figure legend, the reader is referred to the web version of this article.)

3.3. Molecular docking

In order to predict the binding site of LmigOBP1, pentadecanol was chosen to dock with the predicted LmigOBP1 model because of its strong binding affinity with LmigOBP1 (Table 1). The docking result is shown in Fig. 2C. Compared with hexadecanoic acid in the template 2BFH, all the top 20 ligand poses were placed in a similar position. The 20 poses can be divided into two major clusters: (1) polar head group facing the entrance of the protein binding pocket; (2) polar head group facing the bottom of the pocket. The docking pose that was the most representative is shown in Fig. 2E. All the residues with <4.0 Å distances to pentadecanol are represented, including Leu6, Ile10, Leu50, Met54, Phe66, Asn74, Val75, Phe76, Val86, Val87, Cys90, Ile105, Tyr109, Tyr117, Ser118 and Leu119. Among these sixteen amino acid residues, Val87 was found at the bottom of the pentadecanol binding site. The distance from the Asn74 carbonyl oxygen to the hydroxy oxygen of pentadecanol was 3.37 Å, which is suitable for the formation of a hydrogen bond (Fig. 2E).

3.4. Site-directed mutagenesis of LmigOBP1 and binding specificities of mutants

Amino acids were chosen for site-directed mutation on the basis of two criteria: (1) sequence alignment of LmigOBP1 to insect OBPs with validated key binding sites; and (2) molecular docking results of LmigOBP1 bound to pentadecanol. Sequence alignment of several insect OBPs shows that Ser59 of LmigOBP1 was aligned with the key binding site of LUSH, Thr57, which is suggested as a general alcohol-binding site for proteins (Kruse et al., 2003; Thode et al., 2008). The docking experiments suggested that Asn74 forms hydrogen bonds with pentadecanol and Val87, which is located at the bottom of the binding pocket and may affect the length of ligands (Fig. 2E).

Using site-directed mutagenesis, we replaced three residues (Ser59, Asn74 and Val87) with alanine, generating the three mutants S59A, N74A and V87A. The expressed mutant proteins migrated along with LmigOBP1 when analyzed by SDS-PAGE (Fig. 3A). Comparing the CD spectra of LmigOBP1 with the mutant proteins, we found that they all had similar secondary structures. The two minima were around 208 and 222 nm, which are typical of a fold with a majority of α-helical secondary structure (Fig. 3B). Thus, the four PBPs under study displayed a very similar overall fold.

Probed by 1-NPN, the maximum emission wavelengths of mutants S59A, N74A and V87A were of 400–402 nm, similar to LmigOBP1 (400 nm). Saturation binding curves indicated dissociation constants for 1-NPN to mutants S59A, N74A and V87A of 7.76 ± 1.05 μM, 4.45 ± 0.34 μM and 2.52 ± 0.17 μM respectively. LmigOBP1 had a similar dissociation constant of 3.83 ± 0.23 μM.

We investigated the ability of differently sized aliphatic alcohols, from 12- to 16-carbon chain lengths, to displace 1-NPN. The mutant N74A lost almost all efficient binding capacity to the alcohols, dodecanol, tridecanol, tetradecanol, pentadecanol and hexadecanol. None of these alcohols could compete with 50% 1-NPN, even when the ligand concentration reached 20 μM (Fig. 4 and data not shown). In contrast, no differences were found between binding of mutant S59A and LmigOBP1, except for pentadecanol (Table 2). Mutant V87A showed a slightly lower affinity for tridecanol and tetradecanol, but a 3–4-fold decrease in affinity to pentadecanol and hexadecanol, compared to LmigOBP1. Dodecanol did not compete with 50% 1-NPN for mutant V87A, even at 20 μM concentration (Fig. 4 and data not shown).

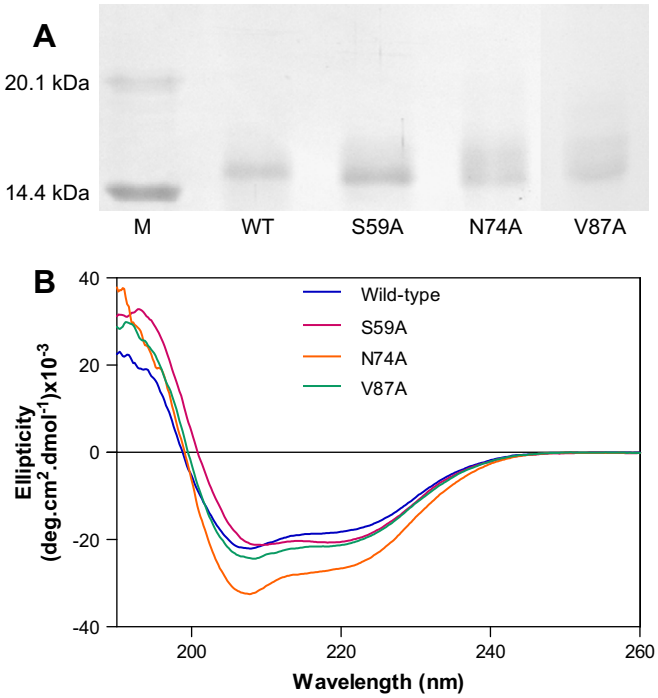

Fig. 3. Recombinant protein characterizations of LmigOBP1 and mutants. (A) 14% SDS-PAGE gel analysis of purified LmigOBP1 wild-type (WT) and mutants S59A, N74A and V87A. (B) CD spectra of LmigOBP1 wild-type (blue), S59A (red), N74A (orange) and V87A (green) mutants. Spectra were recorded in 50 mM Na phosphate, pH 7.4, at 25 °C between 190 and 260 nm. Data are an average of three independent measurements. (For interpretation of the references to colour in this figure legend, the reader is referred to the web version of this article.)

4. Discussion

In this study, we measured the ligand-binding specificity of LmigOBP1 by fluorescence assays with 67 compounds including aliphatic alcohols, ketones, aldehydes, esters and acid, as well as orbicular, heterocyclic and aromatic compound derivatives. Our goal was to understand the physiological function of LmigOBP1 on the basis of ligand affinities. In combination with site-directed mutagenesis and fluorescence binding assays, we discovered that Asn74 from LmigOBP1 is a key binding site involved in the initial recognition of pentadecanol.

Since LmigOBP1 is the only OBP reported in locust, apart from a few isoforms (Ban et al., 2003; Yu et al., 2007), it is surprising to find that none of the volatiles in the feces of locusts were identified as putative pheromones, nor did several plant leaf volatiles exhibit measurable affinity for LmigOBP1. However, LmigOBP1 displayed significant specificity to linear aliphatic alcohols and ketones of approximately 15-carbon chain length. Binding assays with the PBPs MbraPBP1, ApolPBP1 and *Lymantria dispar* PBP suggested that PBPs bind a variety of ligands that are structurally related to pheromones (Campannacci et al., 2001; Bette et al., 2002; Honson et al., 2003), and a honeybee OBP *A. mellifera* L. ASP2 shows a broad binding spectra for various floral ligands (Briand et al., 2001), so LmigOBP1 displays similar ligand-binding specificity as a PBP. This may explain why LmigOBP1 did not bind with plant volatiles from corn or wheat (Konstantopoulou et al., 2004; Shibamoto et al., 2007).

Behaviorally important ligands are unknown in locusts. Though a few locust fecal volatiles, such as 2,5-dimethylpyrazine, can arouse strong electrophysiological responses (Yu et al., 2007), behavior tests have not confirmed their physiological functions. In this study, an aliphatic alcohol pentadecanol and three aliphatic ketones 2-pentadecanone, 2-hexadecanone and 2-heptadecanone

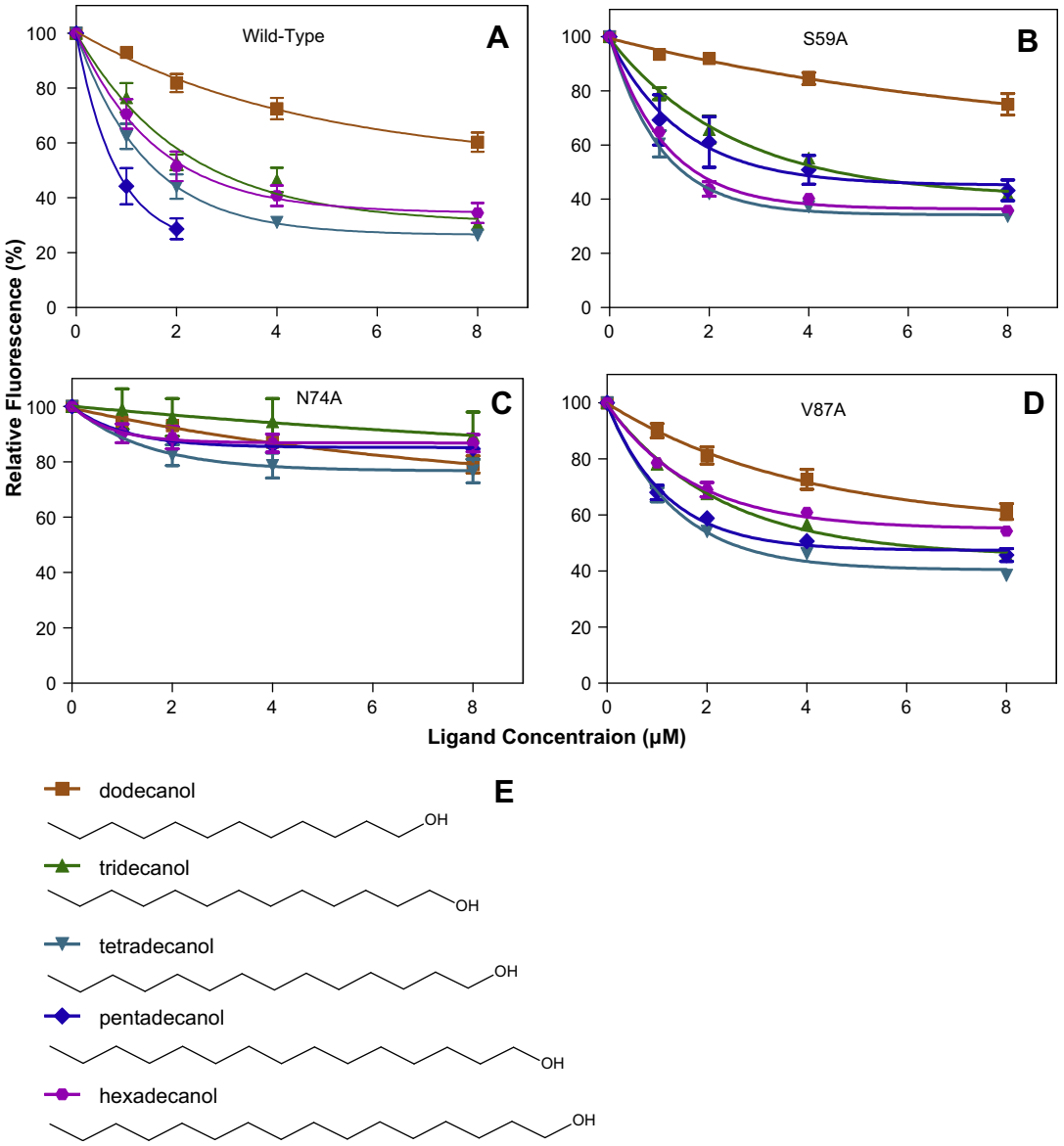

Fig. 4. Comparison of the binding properties of LmigOBP1 wild-type (A) and mutants S59A (B), N74A (C), V87A (D). Each ligand was incubated with 2 μM OBP and 2 μM 1-NPN at increasing concentrations. Fluorescence intensity values were normalized and plotted against total ligand concentration. All spectra were subjected to background subtraction. Data are an average of three independent measurements and the error bars represent the standard deviations of the mean derived from the differences between the measurements. Structures of ligands dodecanol, tridecanol, tetradecanol, pentadecanol and hexadecanol (E) were plotted by ChemSketch.

show high binding affinities (0.58–0.68 μM). The compounds 2-pentadecanone and 2-hexadecanone are known to be produced by the ant *Cataglyphis bicolor*, a natural enemy of locusts (Gökçen et al., 2002). Therefore, LmigOBP1 may perceive interspecies semiochemicals.

Table 2
Binding affinities of aliphatic alcohols to LmigOBP1 Wild-type and mutants. Values are means of three independent experiments.

Ligands	K_i (μM)			
	Wild-type	S59A	N74A	V87A
Dodecanol (C12)	7.20 ± 1.26	8.56 ± 1.85	–	–
Tridecanol (C13)	3.48 ± 1.35	3.37 ± 0.67	–	3.02 ± 0.93
Tetradecanol (C14)	1.30 ± 0.18	1.61 ± 0.17	–	1.54 ± 0.08
Pentadecanol (C15)	0.59 ± 0.19	3.01 ± 1.53	–	1.96 ± 0.04
Hexadecanol (C16)	1.70 ± 0.37	1.77 ± 0.24	–	7.18 ± 3.70

Ligands concentration >20 μM for half-maximal relative fluorescence intensity was represented as "–".

A CHARMm-based docking program CDOCKER was employed to generate a potential binding mode between LmigOBP1 and the ligand pentadecanol. For ligands with eight or more rotatable bonds, CDOCKER can generate more accurate results than other docking programs, so CDOCKER was suitable for our receptor-ligand system (Jon et al., 2004). Docking experiments suggest that the binding cavity is mainly formed by hydrophobic amino acids, including Leu6, Ile10, Leu50, Met54, Phe66, Val75, Phe76, Val86, Val87, Ile105 and Leu119, with the addition of several hydrophilic amino acids, Asn74, Cys90, Tyr109, Tyr117, and Ser118. The hydrophobic amino acid residues are clearly inclined to form van der Waals interactions with ligands. Although Tyr109 and Tyr117 are hydrophilic, they can also form hydrophobic interactions with ligands because of their benzene rings. However, the hydrophilic amino acid Asn74 at the entrance of the binding cavity is very likely involved in the initial recognition of pentadecanol through hydrogen bonding.

Fluorescence binding assays reveal that the single amino acid mutation N74A cannot efficiently bind to dodecanol, tridecanol, tetradecanol, pentadecanol or hexadecanol. A possible explanation is that aliphatic alcohols could not be recognized by the mutant and enter in the binding cavity because of the loss of hydrogen bonding. Mutant V87A showed a slight decrease in binding to alcohols, perhaps because of the incapacity of the mutant to establish specific van der Waals interactions. Mutant S59A did not show a significant change in binding abilities to efficiently bound alcohols, which is inconsistent with the general model for alcohol-binding sites in proteins (Kruse et al., 2003). Perhaps the binding mechanism of long chain alcohols is different to that of small alcohols.

Since Sandler et al. (2000) reported a three-dimensional molecular model of PBP in *B. mori*, conformational changes from ligand-binding to ligand-releasing have been discussed for several OBPs (Horst et al., 2001; Kruse et al., 2003). However, the ligand recognition mechanism has not been precisely elucidated. Comparing our results with other reports, we suggest that the hydrophilic amino acids at the opening of the OBP binding cavity contribute to the initial ligand recognition. For instance, Ser56 of BmorPBP (Sandler et al., 2000) and Asn53 of ApolPBP1 (Mohanty et al., 2004), which are also hydrophilic amino acids at the entrance of the binding cavities, are critical binding sites for specific pheromone binding. Moreover, Ser52 and Thr57 of LUSH, which are located at the opening of the binding pocket and form hydrogen bonds with hydroxyl of alcohol, determine the binding specificity of LUSH (Kruse et al., 2003; Thode et al., 2008).

Although the computational LmigOBP1-pentadecanol docking needs to be confirmed by crystal structure of the protein–ligand complex, both binding assays and docking simulations have shed some light on the molecular mechanism in ligand-OBP interactions. In particular, we show that several long chain aliphatic compounds exhibit high binding affinities to LmigOBP1, and confirm a key binding site, Asn74. These results may aid synthesis of ligand analogs capable of inhibiting the protein binding sites. Moreover, it is also hoped that these results may have a far-reaching impact on insect control, through pheromone-based integrated pest management programs.

Acknowledgements

This work was supported by a key grant from the National Natural Science Foundation (30730012) to L. Z. and the State High Technology Development Program (2008AA02Z307) to Z. Z.

References

Altschul, S.F., Gish, W., Miller, W., Myers, E.W., Lipman, D.J., 1990. Basic local alignment search tool. J. Mol. Biol. 215, 403–410.

Ban, L., Scaloni, A., D'Ambrosio, C., Zhang, L., Yan, Y., Pelosi, P., 2003. Biochemical characterization and bacterial expression of an odorant-binding protein from *Locusta migratoria*. Cell. Mol. Life Sci. 60, 390–400.

Bau, J., Martinez, D., Renou, M., Guerrero, A., 1999. Pheromone-triggered orientation flight of male moths can be disrupted by trifluoromethyl ketones. Chem. Senses 24, 473–480.

Bette, S., Breer, H., Krieger, J., 2002. Probing a pheromone binding protein of the silkmoth *Antheraea polyphemus* by endogenous tryptophan fluorescence. Insect Biochem. Mol. Biol. 32, 241–246.

Briand, L., Nespoulous, C., Huet, J.C., Takahashi, M., Pernollet, J.C., 2001. Ligand binding and physico-chemical properties of ASP2, a recombinant odorant-binding protein from honeybee (*Apis mellifera* L.). Eur. J. Biochem. 268, 752–760.

Brooks, B.R., Bruccoleri, R.E., Olafson, B.D., States, D.J., Swaminathan, S., Karplus, M., 1983. CHARMM: a program for macromolecular energy minimization and dynamics calculations. J. Comput. Chem. 4, 187–217.

Campannacci, V., Krieger, J., Bette, S., Strugis, J.N., Lartigue, A., Cambilau, C., Breer, H., Tegoni, M., 2001. Revisiting the specificity of *Mamestra brassicae* and *Antheraea polyphemus* pheromone-binding proteins with a fluorescence binding assay. J. Biol. Chem. 276, 20078–20084.

Du, G., Prestwich, G.D., 1995. Protein structure encodes the ligand binding specificity in pheromone binding proteins. Biochemistry 34, 8726–8732.

Gill, S.C., Hippel, P.V., 1989. Calculation of protein extinction coefficients from amino acid sequence data. Anal. Biochem. 182, 319–326.

Gökçen, O.A., Morgan, E.D., Dani, F.R., Agosti, D., Wehner, R., 2002. Dufour gland contents of ants of the *Cataglyphis bicolor* group. J. Chem. Ecol. 28, 71–87.

Honson, N., Johnson, M.A., Oliver, J.E., Prestwich, G.D., Plettner, E., 2003. Structure-activity studies with pheromone-binding proteins of the gypsy moth, *Lymantria dispar*. Chem. Senses 28, 479–489.

Horst, R., Damberger, F., Luginbühl, P., Güntert, P., Peng, G., Nikonova, L., Leal, W.S., Wüthrich, K., 2001. NMR structure reveals intramolecular regulation mechanism for pheromone binding and release. Proc. Natl. Acad. Sci. U.S.A. 98, 14374–14379.

Jin, X., Brandazza, A., Navarrini, A., Ban, L.P., Zhang, S.G., Steinbrecht, R.A., Zhang, L., Pelosi, P., 2005. Expression and immunolocalization of odorant-binding and chemosensory proteins in locusts. Cell. Mol. Life Sci. 62, 1156–1166.

Jon, A.E., Mehran, J., Daniel, H.R., Richard, A.L., Michal, V., 2004. Lessons in molecular recognition: the effects of ligand and protein flexibility on molecular docking accuracy. J. Med. Chem. 47, 45–55.

Konstantopoulou, M., Krokos, A.F.D., Mazomenos, B.E., 2004. Chemical composition of corn leaf essential oils and their role in the oviposition behavior of *Sesamia nonagrioides* females. J. Chem. Ecol. 30, 2243–2256.

Krieger, J., Breer, H., 1999. Olfactory reception in invertebrates. Science 286, 720–723.

Kruse, S.W., Zhao, R.D., Smith, D.P., Jones, D.N.M., 2003. Structure of a specific alcohol-binding site defined by the odorant binding protein LUSH from *Drosophila melanogaster*. Nat. Struct. Biol. 10, 694–700.

Luthy, R., Bowie, J.U., Eisenberg, D., 1992. Assessment of protein models with three-dimensional profiles. Nature 356, 83–85.

Maida, R., Krieger, J., Gebauer, T., Lange, U., Ziegelberger, G., 2000. Three pheromone-binding proteins in olfactory sensilla of the two silkmoth species *Antheraea polyphemus* and *Antheraea pernyi*. Eur. J. Biochem. 267, 2899–2908.

Maida, R., Ziegelberger, G., Kaissling, K.E., 2003. Ligand binding to six recombinant pheromone-binding proteins of *Antheraea polyphemus* and *Antheraea pernyi*. J. Comp. Physiol. [B] 173, 565–573.

Matsuo, T., Sugaya, S., Yasukawa, J., Aigaki, T., Fuyama, Y., 2007. Odorant-binding proteins OBP57d and OBP57e affect taste perception and host-plant preference in *Drosophila sechellia*. PLoS Biol. 5, 985–996.

Mohanty, S., Zubov, S., Gronenborn, A.M., 2004. The solution NMR structure of *Antheraea polyphemus* PBP provides new insight into pheromone recognition by pheromone-binding proteins. J. Mol. Biol. 337, 443–451.

Pelosi, P., Zhou, J.J., Ban, L.P., Calvello, M., 2006. Soluble proteins in insect chemical communication. Cell. Mol. Life Sci. 63, 1658–1676.

Prestwich, G.D., Du, G., LaForest, S., 1995. How is pheromone specificity encoded in proteins? Chem. Senses 20, 461–469.

Quero, C., Bau, J., Guerrero, A., Renou, M., 2004. Responses of the olfactory receptor neurons of the corn stalk borer *Sesamia nonagrioides* to components of the pheromone blend and their inhibition by a trifluoromethyl ketone analogue of the main component. Pest Manag. Sci. 60, 719–726.

Riba, M., Sans, A., Bau, P., Grolleau, G., Renou, M., Guerrero, A., 2001. Pheromone response inhibitors of the corn stalk borer *Sesamia nonagrioides*. Biological evaluation and toxicology. J. Chem. Ecol. 27, 1879–1897.

Rychaert, J.P., Ciccotti, G., Berendsen, H.J.C., 1977. Numerical integration of the Cartesian equations of motion of a system with constraints: molecular dynamics of n-alkanes. J. Comput. Phys. 23, 327–341.

Sali, A., Blundell, T.L., 1993. Comparative protein modeling by satisfaction of spatial restraints. Mol. Biol. 234, 779–815.

Sandler, B.H., Nikonova, L., Leal, W.S., Clardy, J., 2000. Sexual attraction in the silkworm moth: structure of the pheromone-binding-protein-bombykol complex. Chem. Biol. 7, 143–151.

Shibamoto, T., Horiuchi, M., Umano, K., 2007. Composition of the young green barley and wheat leaves. J. Essent. Oil Res. 19, 134–137.

Steinbrecht, R.A., Laue, M., Ziegelberger, G., 1995. Immunolocalization of pheromone-binding protein and general odorant-binding protein in olfactory sensilla of the silk moths *Antheraea* and *Bombyx*. Cell Tissue Res. 282, 203–217.

Thode, A.B., Kruse, S.W., Nix, J.C., Jones, D.N.M., 2008. The role of multiple hydrogen-bonding groups in specific alcohol binding sites in proteins: insights from structural studies of LUSH. J. Mol. Biol. 376, 1360–1376.

Vogt, R.G., Riddiford, L.M., 1981. Pheromone binding and inactivation by moth antennae. Nature 293, 161–163.

Vogt, R.G., Prestwich, G.D., Lerner, M.R., 1991. Odorant-binding protein subfamilies associate with distinct classes of olfactory receptor neurons in insects. J. Neurobiol. 22, 74–84.

Wu, G., Robertson, D.H., Brooks III., C.L., Vieth, M., 2003. Detailed analysis of grid-based molecular docking: a case study of CDOCKER – a CHARMm-based MD docking algorithm. J. Comput. Chem. 24, 1549–1562.

Xu, P.X., Atkinson, R., Jones, D.N.M., Smith, D.P., 2005. *Drosophila* OBP LUSH is required for activity of pheromone-sensitive neurons. Neuron 45, 193–200.

Yu, Y.X., Cui, X.J., Jiang, Q.Y., Jin, X., Guo, Z.Y., Zhao, X.B., Bi, Y.P., Zhang, L., 2007. New isoforms of odorant-binding proteins and potential semiochemicals of locusts. Arch. Insect Bio. Physiol. 65, 39–49.

Zhang, S.G., Maida, R., Steinbrecht, R.A., 2001. Immunolocalization of odorant-binding proteins in noctuid moths (Insecta, Lepidoptera). Chem. Senses 26, 885–896.